INTERNATIONAL JOURNAL OF PRECISION ENGINEERING AND MANUFACTURING Vol. 15, No. 3, pp. 567-575 MARCH 2014 / 567
DOI: 10.1007/s12541-014-0372-3

Development of a High-Precision Calibration Method for Inertial Measurement Unit

Moon-Sik Kim[1,#], Si-Bok Yu[1], and Kwang-Soo Lee[1]

1 Korea Automotive Technology Institute, 330 Pungse-ro, Pungse-myeon, Dongnam-gu, Cheonan, South Korea, 330-912
Corresponding Author / E-mail: mskim@katech.re.kr, TEL: +82-041-559-3099, FAX: +82-041-559-3237

KEYWORDS: MEMS, Accelerometer, Gyroscope, Coning angle, Azimuth angle

MEMS (Micro-Electromechanical Systems) based IMU (Inertial Measurement Unit) including accelerometers and gyroscopes is widely used for various applications such as INS (Inertial Navigation System), pose estimation devices and others for many industries such as toy, medical, automotive and military industry. But MEMS sensor chip originally has bias and sensitivity errors from manufacturing, and there is also axis misalignment when mounting a MEMS chip on IMU PCB layer. These error factors cause inaccuracy measurement results and non-linear measurement characteristics of IMU. In this paper, accelerometers and gyroscopes are mathematically modeled based on these error factors including bias, sensitivity, coning angle and azimuth angle. Calibration procedures for accelerometers and gyroscopes are formulated using nonlinear Gauss-Newton regression logic. The effectiveness of the proposed calibration procedures are proven by simulation and experiment using high accuracy 2-axis rotational gimbal motion system.

Manuscript received: September 17, 2013 / Revised: December 20, 2013 / Accepted: January 20, 2014

NOMENCLATURE

C = coning angle
A = azimuth angle
B = bias
S = sensitivity
V= output value of the sensor

1. Introduction

Currently, there are in market many IMU products from low-price products to high-price military products. These are used for various purposes such as toys, GPS-INS integration systems, pose estimation units and others. But especially, low cost IMUs show large measurement errors because it is not calibrated efficiently. In general, IMU consists of multiple axis accelerometers and gyroscopes based on MEMS.

Benjamin P. proposed the automatic calibration system for the accelerometers and gyroscopes by 3-axis manipulation system. The sensor model accounts for scale, misalignment, non-orthogonally and bias errors.[1] Chan L. developed the calibration method for the accelerometers and gyroscopes by unscented Kalman filter (UKF),[2] Bonnet S. proposed the calibration method for low-cost inertial sensors.[3] Keeyoung C. used pendulum motion for IMU calibration.[4] In the case of inertial navigation system (INS), Kyungjun H. developed the calibration method optimized for INS.[5] To calibrate strap down MEMS IMU sensors, the Kalman filter based estimation calibration method is proposed.[6] In traditional method, the mathematical model including only bias and scale factors is used for IMU calibration.[7]

In this paper, 3-axis accelerometer and gyroscope characteristics are mathematically parameterized. These parameters are considered in all axes. Gravity sensing accelerometer calibration, as well as angular rate sensing gyroscope calibration, can be mathematically described by a nonlinear algebraic relationship. Proposed sensor calibration method uses an iterative Gauss-Newton numeric solution strategy. These calibration methods were tested with simulation and experiment data and found to be reliable and accurate. Gravity sensing accelerometer based attitude construction is also described mathematically with a nonlinear algebraic relationship. Here, an analytic closed-form solution for the attitude construction is presented, as well as a Gauss-Newton iterative solution.

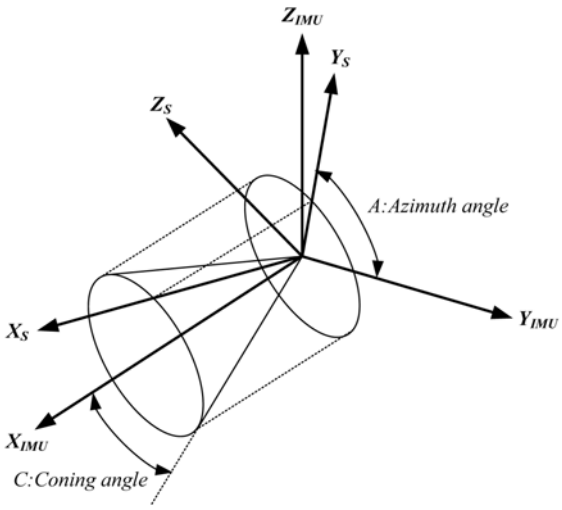

Fig. 1 Coning and azimuth angle description

2. Sensor Modeling

Misalignment between the IMU fixed axes and the sensor fixed axes can exist due to attachment and mounting inaccuracy associated with internal sensor manufacturing inaccuracies. Here, sensor fixed axes refer to the internal sensing axes of the sensor. Such misalignment will be described by the coning angle (C) and azimuth angle (A). Fig. 1 illustrates the definition of these two misalignment angles for the case the desired measurement axis and the true measurement axis. Coning angle is defined as the angle subtended by the desired and true measurement axes. A cone shape is created when the excitation axis is rotated about the desired axis. To define the azimuth angle, consider projecting the cone and excitation axis onto the Y_{IMU}-Z_{IMU} plane. The projected shape is a circle with a radial marking. Azimuth angle is defined as the angle subtended by the Z_{IMU} axis and projected excitation axis. The internal sensor fixed excitation axes relative to the IMU axes can be defined by a rotational transformation associated with the coning and azimuth angles. This transformation is geometrically defined by 1) heading (A) around the circle w.r.t Y_{IMU}, and 2) spin (C) w.r.t the heading radial. Other important parameters associated with the sensor behavior are bias (B) and sensitivity (S). A systematic deviation exhibited by a measurement value from a reference value is defined as bias. Further, sensitivity is defined as the ratio of observed output signal produced with respect to a specified unit of sensor input change.

2.1 Accelerometer equations

With the geometry described in Fig. 1, the gravitational acceleration vector expressed in the gimbal frame described in experiment chapter is

$$\boldsymbol{G}_i = \begin{bmatrix} g & 0 & 0 \end{bmatrix}^T \tag{1}$$

where, g denotes the local value of gravity. $\boldsymbol{G_i}$ is considered to be the known reference vector.

Extraction of the complete yaw-pitch-roll orientation state from a gravity vector measurement scheme employing a single accelerometer sensor package is feasible. The gravitational acceleration vector expressed in inertial axis is obtained by combining the Euler transformation which is the yaw-pitch-roll orientation.

The Euler transformation is described as below

$$\boldsymbol{T}_{body} = Rot(x,\phi)Rot(y,\theta)Rot(z,\varphi) \tag{2}$$

Now consider effects from misalignment errors due to the azimuth and coning angles in the IMU. The following analysis must be conducted individually for each measurement axis. First consider the X_{IMU} axis as the desired measurement axis. A sequential transformation consisting first of azimuth rotation A_x w.r.t x leading to a second intermediate frame, and next of coning rotation C_x w.r.t the intermediate y axis which leads to the true measurement or sensor fixed reference frame associated with x is implemented.

$$T_{Ax} = \begin{bmatrix} 1 & 0 & 0 \\ 0 & cosA_x & sinA_x \\ 0 & -sinA_x & cosA_x \end{bmatrix}, \quad T_{Cx} = \begin{bmatrix} cosC_x & 0 & -sinC_x \\ 0 & 1 & 0 \\ sinC_x & 0 & cosC_x \end{bmatrix} \tag{3}$$

$$T_{Ay} = \begin{bmatrix} cosA_y & 0 & -sinA_y \\ 0 & 1 & 0 \\ sinA_y & 0 & cosA_y \end{bmatrix}, \quad T_{Cy} = \begin{bmatrix} cosC_y & sinC_y & 0 \\ -sinC_y & cosC_y & 0 \\ 0 & 0 & 1 \end{bmatrix} \tag{4}$$

$$T_{Az} = \begin{bmatrix} cosA_z & sinA_z & 0 \\ -sinA_z & cosA_z & 0 \\ 0 & 0 & 1 \end{bmatrix}, \quad T_{Cz} = \begin{bmatrix} 1 & 0 & 0 \\ 0 & cosC_z & sinC_z \\ 0 & -sinC_z & cosC_z \end{bmatrix} \tag{5}$$

The calibration matrix is calculated as below.

$$T_{sn\_x} = T_{Cx}T_{Ax} = \begin{bmatrix} cosC_x & sinA_xsinC_x & -cosA_xsinC_x \\ 0 & cosA_x & sinA_x \\ sinC_x & -sinA_xcosC_x & cosA_xcosC_x \end{bmatrix} \tag{6}$$

$$T_{sn\_y} = T_{Cy}T_{Ay} = \begin{bmatrix} cosA_ycosC_y & sinC_y & -sinA_ycosC_y \\ -cosA_ysinC_y & cosC_y & sinA_ysinC_y \\ sinA_y & 0 & cosA_y \end{bmatrix} \tag{7}$$

$$T_{sn\_z} = T_{Cz}T_{Az} = \begin{bmatrix} cosA_z & sinA_z & 0 \\ -sinA_zcosC_z & cosA_zcosC_z & sinC_z \\ sinA_zsinC_z & -cosA_zsinC_z & cosC_z \end{bmatrix} \tag{8}$$

The integrated calibration matrix T_{sn} is composed with first, second and third rows each of T_{sn_x}, T_{sn_y} and T_{sn_z}.

$$\boldsymbol{T_{sn}} = \begin{bmatrix} T_{sn\_x}(1,;) \\ T_{sn\_y}(1,;) \\ T_{sn\_z}(1,;) \end{bmatrix} = \begin{bmatrix} cosC_x & sinA_xsinC_x & -cosA_xsinC_x \\ -cosA_ysinC_y & cosC_y & sinA_ysinC_y \\ sinA_zsinC_z & -cosA_zsinC_z & cosC_z \end{bmatrix} \tag{9}$$

Therefore, accelerometer with misalignment in coning an azimuth angle outputs acceleration values G_{body} according to the Euler transformation.

$$\boldsymbol{G_{body}} = \boldsymbol{T_{sn}}\,\boldsymbol{T_{body}}\,\boldsymbol{G_i} \tag{10}$$

Assume the each axis of accelerometer has bias and sensitivity.

$$\boldsymbol{B} = \begin{bmatrix} b_x & b_y & b_z \end{bmatrix}^T \tag{11}$$

The final output value of accelerometer is like below.

$$\boldsymbol{V_a} = \boldsymbol{B} + \boldsymbol{s} \cdot \boldsymbol{G_{body}} = \boldsymbol{B} + \boldsymbol{s} \cdot \boldsymbol{T_{sn}} \cdot \boldsymbol{T_{body}} \cdot \boldsymbol{G_i} \tag{12}$$

2.2 Gyroscope Equations

With the geometry described in Fig. 1, the angular velocity vector of the model expressed in the model fixed reference frame is

$$\boldsymbol{\Omega_{sn}} = \left[\Omega_x\ \Omega_y\ \Omega_z\right]^T \tag{13}$$

Ω_{sn} is considered to be a known vector produced by the gyroscopes. Extraction of the complete yaw-pitch-roll orientation state from an angular rate measurement and integration scheme employing a single gyroscope sensor package is feasible. By relating these measured angular rate components with the temporal rates of changes of Euler rotation angles, the full angular state can be determined.

Based on the yaw-pitch-roll rotation sequence, the angular velocity vector can be built-up from the component rotation rates, or

$$\boldsymbol{\Omega_{sn}} = T_{m2}\dot{\phi} + T_m\dot{\phi} + I\dot{\varphi} = \begin{bmatrix}\Omega_x\\ \Omega_y\\ \Omega_z\end{bmatrix} = \begin{bmatrix}\dot{\theta}\sin\varphi + \dot{\phi}\cos\varphi\cos\theta\\ \dot{\theta}\cos\varphi - \dot{\phi}\cos\theta\sin\varphi\\ \dot{\varphi} + \dot{\phi}\sin\theta\end{bmatrix} \tag{14}$$

where, $T_{m2} = Rot(z,\ \varphi)Rot(y,\ \theta)$, $T_m = Rot(z,\ \varphi)$

Euler yaw rate $\dot{\varphi}$ is executed w.r.t the first intermediate Z_S axis, Euler pitch rate $\dot{\theta}$ is executed w.r.t Y_S axis, and Euler roll rate $\dot{\phi}$ is executed w.r.t X_S axis.

The bias, sensitivity, coning and azimuth angle transformation matrix are described similar to accelerometer equations. The final output value of gyroscope is like below

$$\boldsymbol{V_g} = \boldsymbol{B} + \boldsymbol{s} \cdot \boldsymbol{T_{sn}} \cdot \boldsymbol{\Omega} \tag{15}$$

3. Sensor Calibration

In order to get the calibration parameters including bias (b_x, b_y, b_z), sensitivity (s_x, s_y, s_z), coning angle (C_x, C_y, C_z) and azimuth angle (A_x, A_y, A_z), a Gauss-Newton iterative nonlinear regression method is used. Represent the accelerometer sensor relationships as

$$V = F(B,S,A,C,\phi,\theta,\varphi,g) \tag{16}$$

where, function F denotes the nonlinear function. The right-hand side of this equation can also be expanded in a Taylor series about a reference solution.

$$V = V_r + \frac{\partial F(X,P)}{\partial X}_r (X - X_r) + \ldots \tag{17}$$

where, $X = [B\ \ S\ \ C\ \ A]^T$, $\dfrac{\partial F(X,P)}{\partial X} = \left[\dfrac{\partial F}{\partial B}\dfrac{\partial F}{\partial S}\dfrac{\partial F}{\partial C}\dfrac{\partial F}{\partial A}\right]$, $P = [\phi\ \ \theta\ \ \varphi\ \ g]$.

X denotes a vector containing the unknown variables, and P denotes a vector of known parameters. Suppose initial estimates for the bias, sensitivity, azimuth, and coning variables are known and interpreted to be the reference solution X_r. More detailed partial derivatives are described in Annex.

$$X = X_r + \left(\frac{\partial F(X,P)}{\partial X_r}^T \frac{\partial F(X,P)}{\partial X_r}\right)^{-1} \frac{\partial F(X,P)}{\partial X_r}^T (V - V_r) \tag{18}$$

Eq. (18) represents the iterative Gauss-Newton regression algorithm and includes the cost function. X is computed form Eq. (18) and reinterpreted as the reference solution for the next computation cycle. This process is repeated until the cost value is less than solution tolerance. The cost function of this method is defined as

$$CF(.) = \left\{\left(\frac{\partial F(X,P)}{\partial X_r}^T \frac{\partial F(X,P)}{\partial X_r}\right)^{-1} \frac{\partial F(X,P)}{\partial X_r}^T (V - V_r)\right\}^2 \tag{19}$$

For apply calculated calibration variables, in case of accelerometer

$$\begin{gathered}(s \cdot T_{sn})^{-1}(V - B) = T_{body} G_i = V_{true}\\ V_{true} = T_{sn}^{-1} s^{-1}(V - B)\end{gathered} \tag{20}$$

where, $\mathbf{V_{true}}$ is calibrated acceleration value. For real-time acceleration measurement, Eq. (25) is conducted in real-time. In-case of gyroscope,

$$\begin{gathered}(s \cdot T_{sn})^{-1}(V - B) = \Omega = V_{true}\\ V_{true} = T_{sn}^{-1} s^{-1}(V - B)\end{gathered} \tag{21}$$

4. Simulation

The Gauss-Newton regression algorithms for accelerometers and gyroscopes calibration are validated with synthetically generated data using MATLAB. This data is intended to represent actual data that would be collected from hardware using high accuracy 2-axis gimbal motion system.

4.1 Accelerometer sensor calibration

In case of accelerometers simulation, pitch and yaw angle movement from 0 deg to 90 deg is conducted as ramp movement during 90 seconds. Because of the high precision 2-axis gimbals used in the experiment, only 2-axis movement is also applied in the simulation. The initial condition of the IMU related with mounting direction on the gimbals is same to the experimental condition.

The left side in Fig. 2 shows the Euler angles of 2-axis, and the right side shows output of accelerometers at this time. The assumption values of bias, sensitivity, coning and azimuth angle are shown in Table 1. The simulation result by the proposed method is shown in Table 2 showing the effectiveness of the proposed algorithm.

4.2 Gyroscope calibration

Similar to the accelerometers simulation, the gyroscopes simulation is conducted in the same condition with the experimental condition. Only 2-axis angular velocity is applied to gyroscopes. To remove the jerk problem, the sinusoid angular velocity profile is used. Eq. (22) shows the applied sinusoid functions to the roll and pitch axis in simulation and experiment.

$$\begin{gathered}\phi(t_i) = \theta(t_i) = amp \cdot cos(freq \cdot 2\pi \cdot t_i)\\ \dot{\phi}(t_i) = \dot{\theta}(t_i) = -amp \cdot freq \cdot 2\pi sin(freq \cdot 2\pi \cdot t_i) \quad 0 \le t \le 10\text{sec}\end{gathered} \tag{22}$$

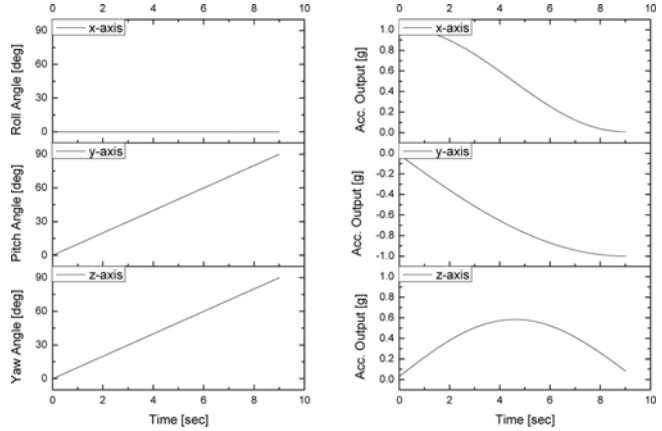

Fig. 2 Calculated angle input and accelerometer output

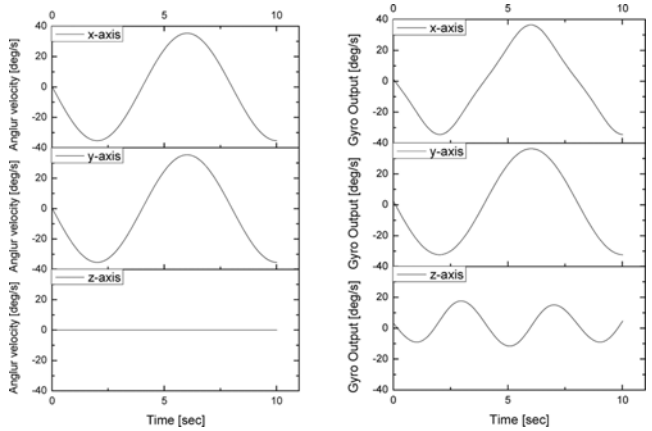

Fig. 3 Calculated angular velocity input and gyroscope output

Table 1 Assumption of accelerometer parameters for simulation

Axis	bias [g]	sensitivity	coning angle [rad]	azimuth angle [rad]
x	0.0100	1.0100	0.0010	0.0012
y	0.0200	1.0200	0.0026	0.0026
z	0.0300	1.0300	0.0019	0.0023

Table 2 Accelerometer simulation result (parameter estimation errors)

Axis	bias [g]	sensitivity	coning angle [rad]	azimuth angle [rad]
x	-1.5959×10^{-16}	2.2204×10^{-16}	-4.7198×10^{-5}	-2.1730×10^{-5}
y	-2.6368×10^{-16}	-2.2204×10^{-16}	-1.7994×10^{-5}	-1.7994×10^{-5}
z	0	0	-1.9862×10^{-5}	3.1072×10^{-5}

Table 3 Assumption of gyroscope parameters for simulation

Axis	bias [rad/s]	sensitivity	coning angle [rad]	azimuth angle [rad]
x	0.0175	1.0033	0.0175	0.0262
y	0.0349	1.0066	0.0349	0.0436
z	0.0524	1.0099	0.0524	0.0611

Table 4 Gyroscope simulation result (parameter estimation errors)

Axis	bias [rad/s]	sensitivity	coning angle [rad]	azimuth angle [rad]
x	0.3469×10^{-17}	0	0	0.4996×10^{-15}
y	0.6939×10^{-17}	0	0.4857×10^{-16}	0.1249×10^{-12}
z	0	0	0	0

where, *amp* = 45 deg, *freq* = 0.125 sec and sampling time is 20 msec.

The left side in Fig. 3 shows the Euler angle velocity profile used in this simulation. The right side in Fig. 3 shows the 3-axis gyroscopes. The simulation result in Table 4 also shows the effectiveness of the proposed algorithm.

5. Experiment

For experimental verification, high accuracy 2-axis gimbal motion system is used. In this paper, AOM300-200 model manufactured by AEROTECH Corp. is used for 2-axis high accuracy rotational movement. In order to compare between the simulation results with the experiment results, 2-axis rotational movement condition is configured same as MATLAB simulation. The IMU used in this experiment is ADXL16505 which includes 3-axis accelerometer, 3-axis gyroscope and 3-axis magnetometer of Analog Device Corp. In order to help accelerometer measuring gravity in stability, pitch and yaw axis are driven with the constant angular velocity 1deg/s. In case of gyroscope, various angular velocities must be required for calibrating the sensor. To eliminate jerk problem, the sigmoid function is used to drive motion system. Fig. 4 shows the description of the sensor and motion axis. The dotted lines are the motion axis of AOM300-200. X, Y and Z indicate the axis of ADXL 16505 IMU.

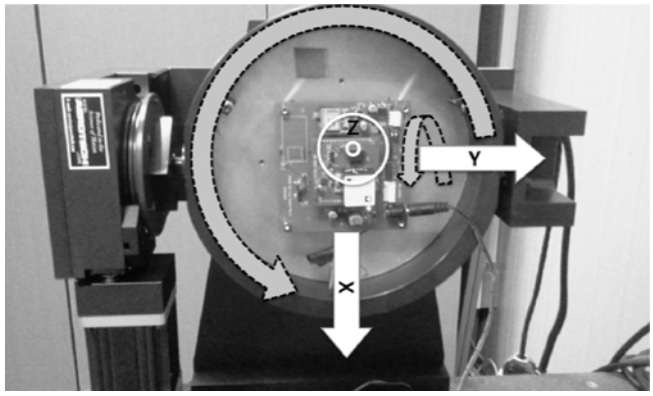

Fig. 4 ADXL 16505 and AOM300-200

Table 5 Accelerometer calibration experiment results

Axis	bias [g]	sensitivity	coning angle [rad]	azimuth angle [rad]
x	0.0314	1.0023	-0.0318	0.7667
y	0.0406	1.0112	-0.0350	0.9855
z	0.0498	0.9905	-0.0174	0.0958

5.1 Accelerometer calibration

The calibration results of accelerometers are shown from Fig. 5 to Fig. 16. Fig. 5, 9 and 13 show the full scale graph for 90 sec. The calibrated results are good in most acceleration range from 0 to 9.8 m/s^2. The applied acceleration to sensor is the gravity, so the calibration range is limited in 1 g. Table 5 shows calibration parameters. As shown

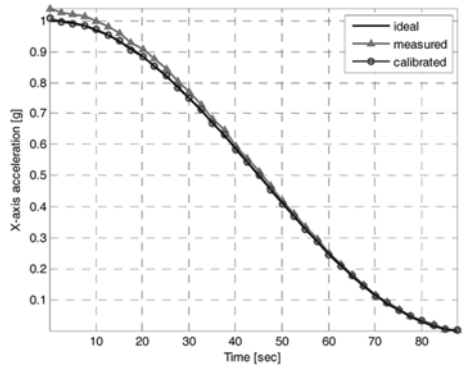

Fig. 5 X-axis accelerometer calibration result (full scale)

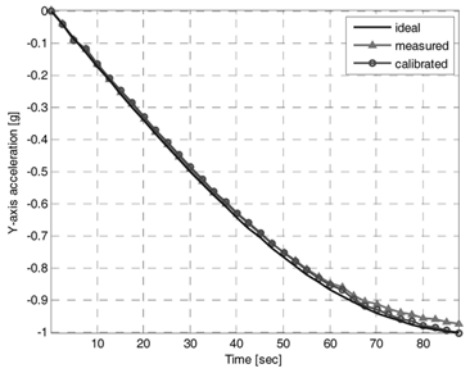

Fig. 9 Y-axis accelerometer calibration result (full scale)

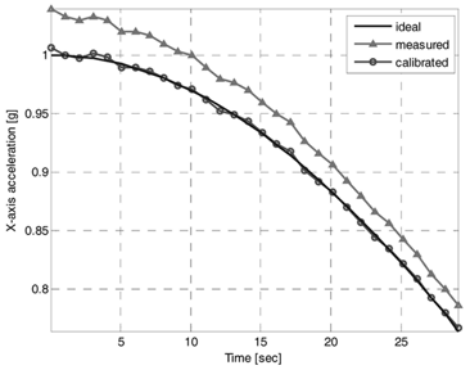

Fig. 6 X-axis accelerometer calibration result (0~30 sec)

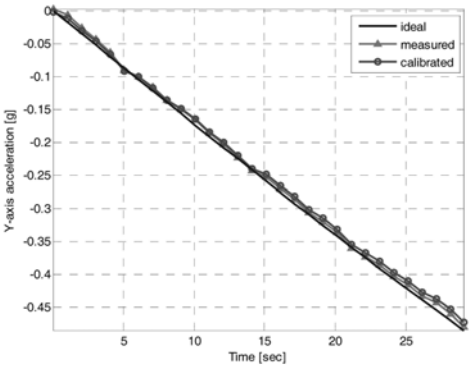

Fig. 10 Y-axis accelerometer calibration result (0~30 sec)

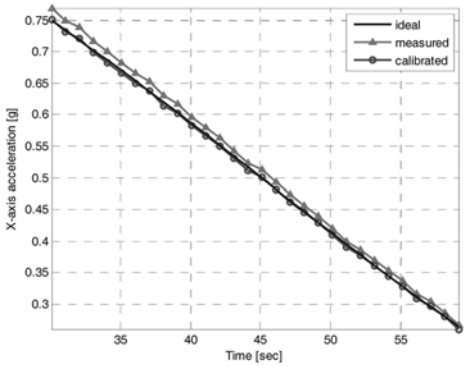

Fig. 7 X-axis accelerometer calibration result (30~60 sec)

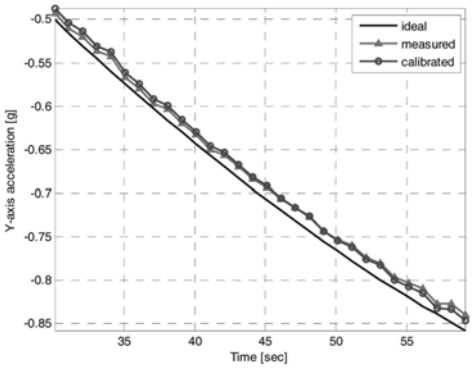

Fig. 11 Y-axis accelerometer calibration result (30~60 sec)

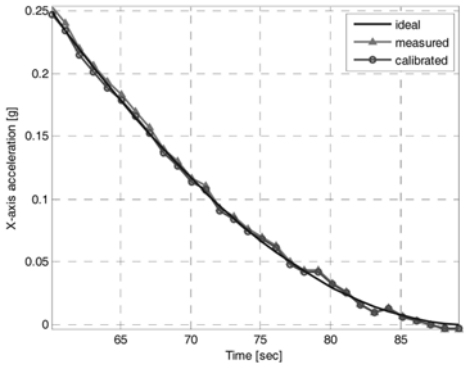

Fig. 8 X-axis accelerometer calibration result (60~90 sec)

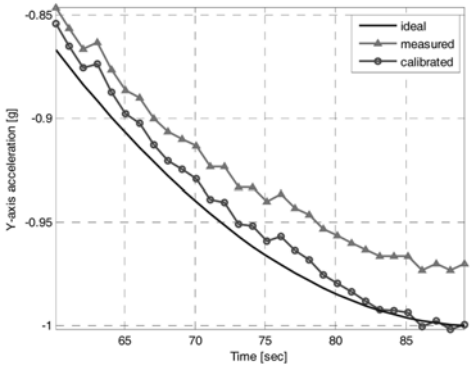

Fig. 12 Y-axis accelerometer calibration result (60~90 sec)

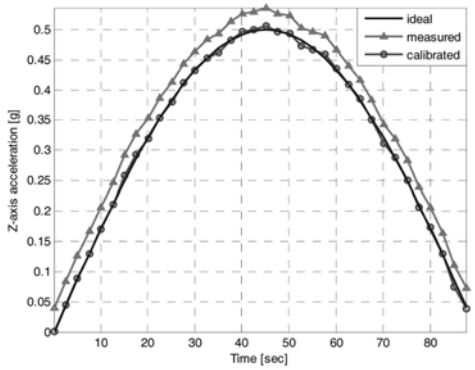

Fig. 13 Z-axis accelerometer calibration result (full scale)

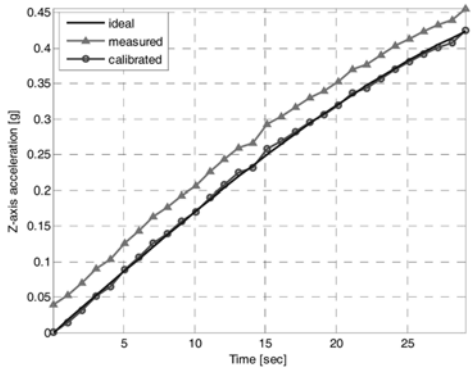

Fig. 14 Z-axis accelerometer calibration result (0~30 sec)

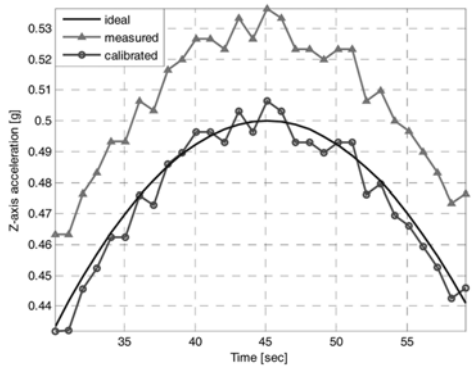

Fig. 15 Z-axis accelerometer calibration result (30~60 sec)

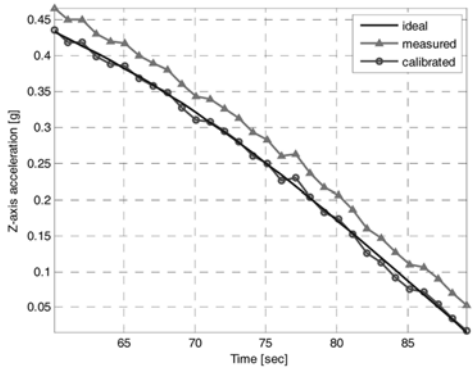

Fig. 16 Z-axis accelerometer calibration result (60~90 sec)

Table 6 Gyroscope calibration experiment results

Axis	bias [rad/s]	sensitivity	coning angle [rad]	azimuth angle [rad]
x	0.000061941	0.9861	0.0140	-0.4086
y	0.00020552	1.0352	0.0109	-0.6834
z	0.00036160	0.9977	-0.0172	0.5422

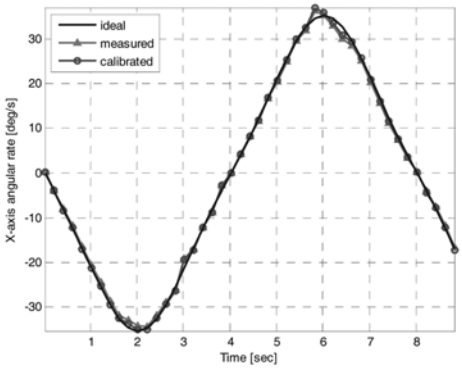

Fig. 17 X-axis gyroscope calibration result (full scale)

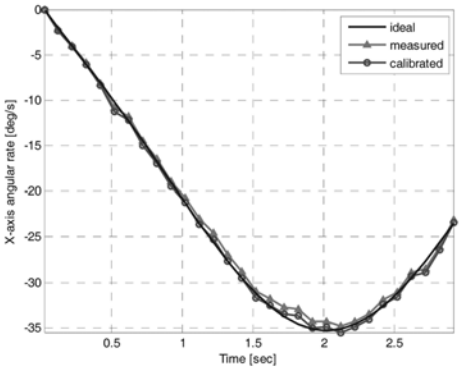

Fig. 18 X-axis gyroscope calibration result (0~30 sec)

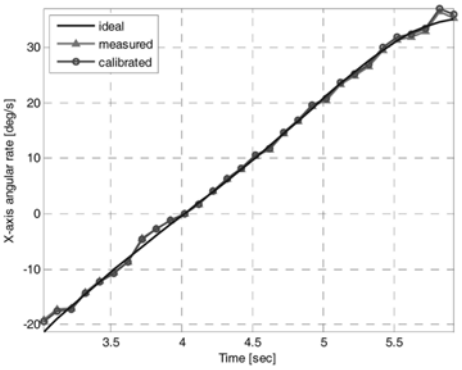

Fig. 19 X-axis gyroscope calibration result (30~60 sec)

in result graphs, calibration is conducted well with non-linear characteristics produced by coning and azimuth calibration factor.

5.2 Gyroscope calibration

From Fig. 17 to 28, the gyroscope calibration result graphs are shown. In similar to acceleration results, the calibration gyroscope result is close

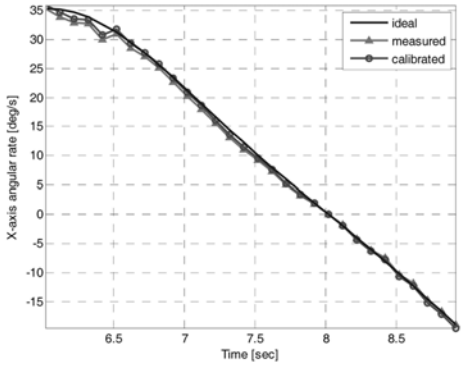

Fig. 20 X-axis gyroscope calibration result (60~90 sec)

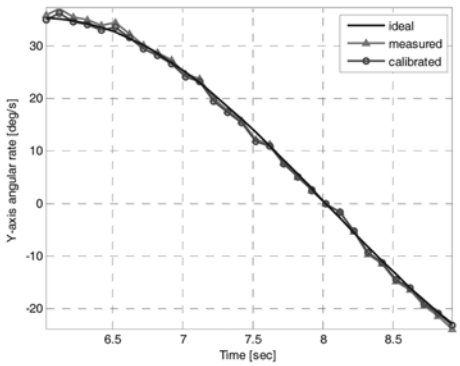

Fig. 24 Y-axis gyroscope calibration result (60~90 sec)

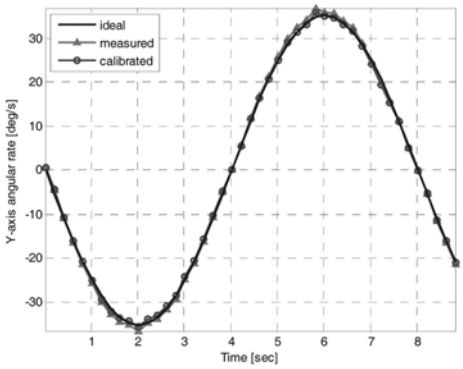

Fig. 21 Y-axis gyroscope calibration result (full scale)

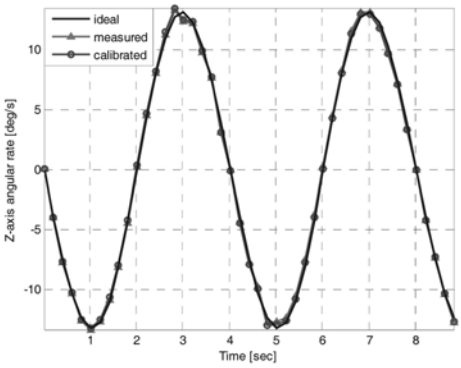

Fig. 25 Z-axis gyroscope calibration result (full scale)

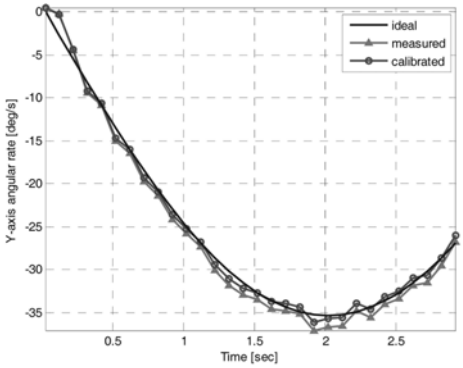

Fig. 22 Y-axis gyroscope calibration result (0~30 sec)

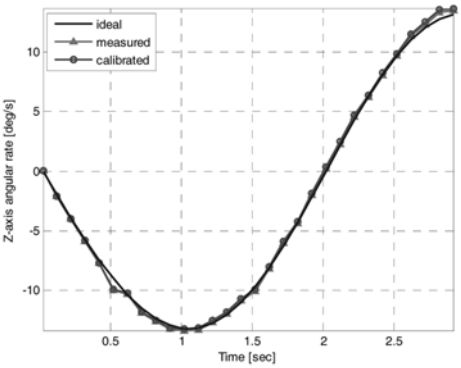

Fig. 26 Z-axis gyroscope calibration result (0~30 sec)

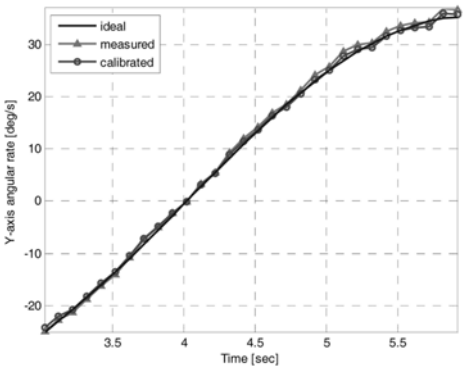

Fig. 23 Y-axis gyroscope calibration result (30~60 sec)

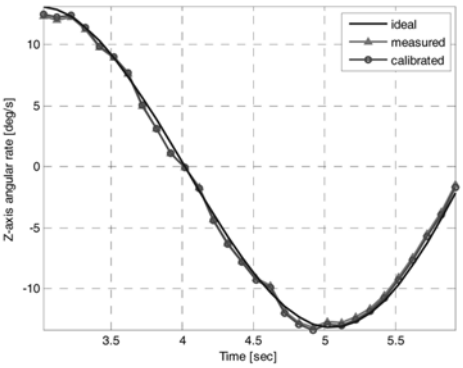

Fig. 27 Z-axis gyroscope calibration result (30~60 sec)

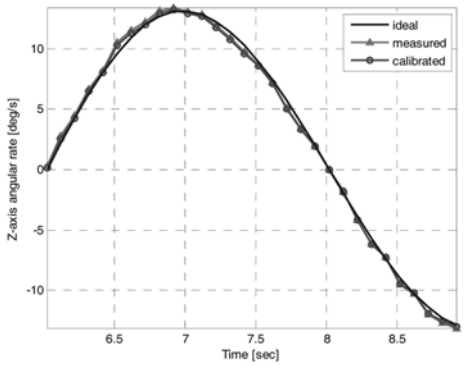

Fig. 28 Z-axis gyroscope calibration result (60~90 sec)

to the ideal rotational velocity line.

6. Conclusion

In this paper, the calibration method for IMU including multi-axis accelerometers and gyroscopes is proposed and verified through simulation and experiments.

A general analytical framework describing mathematical relationships between 3-axis gravitational acceleration and angular rate data to the test article yaw, pitch and roll states is developed. For calibration and angle calculation of accelerometer package and calibration of gyroscope package, Gauss-Newton iteration method is used. These procedures are also tested with simulated data without noise and found to be highly accurate. Specially, the high accuracy 2-axis gimbals motion system is used to verify the proposed algorithm in experiment. If the proposed algorithm is used in various application products using the IMU, it is proven not only through simulation but also experiments.

ACKNOWLEDGEMENT

This research was supported by the Ministry of Trade, Industry and Energy, Korea, under the project 10043352 supervised by the Korea Evaluation Institute of Industrial Technology and R0001230 supervised by the Korea Institute for the Advancement of Technology.

REFERENCES

1. Benjamin, P., "Development of an Automatic IMU Calibration System," ETH Master Thesis, 2013.
2. Li, C., Zhang, S., and Cao, Y., "One New Onboard Calibration Scheme for Gimbaled IMU," Measurement, Vol. 46, No. 8, pp. 2359-2375, 2013.
3. Bonnet, S., Bassompierre, C., Godin, C., Lesecq, S., and Barraud, A. "Calibration Methods for Inertial and Magnetic Sensors, Sensors and Actuator A: Physical," Vol. 156, No. 2, pp. 302-311, 2009.
4. Choi, K., Jang, S., and Kim, Y., "Calibration of Inertial Measurement Units Using Pendulum Motion," International Journal of Aeronautical and Space Sciences, Vol. 11, No. 3, pp. 234-239, 2010.
5. Han, K. J., Park, B. S., Lee, S. W., and Yu, M. J., "Accurate Calibration Method for SDINS Incorporating Earth-Rate Injection Technique," Proc. of 12th International Conference on Control, Automation and Systems, pp. 2100-2105, 2012.
6. Aydemir, G. A. and Saranli, A., "Characterization and Calibration of MEMS Inertial Sensors for State and Parameter Estimation Applications," Measurement, Vol. 45, No. 5, pp. 1210-1225, 2012.
7. Lee, D., lee, S., Park, S., and Ko, S., "Test and Error Parameter Estimation for MEMS - based Low Cost IMU Calibration," Int. J. Precis. Eng. Manuf., Vol. 12, No.4, pp.597-603, 2011.

ANNEX

For completeness of Gauss-Newton algorithm, partial derivatives of Eqs. (12) and (15) are given below. For x-axis accelerometer, partial derivatives are as follows.

$$\frac{\partial V_{ax}}{\partial B} = 1 \tag{A.1}$$

$$\frac{\partial V_{ax}}{\partial S} = g \cdot (cosC_x cos\theta cos\varphi - cosA_x sinC_x (sin\phi cos\varphi + cos\phi sin\theta cos\varphi) - sinA_x sinC_x (cos\phi sin\varphi - sin\phi sin\theta cos\varphi) \tag{A.2}$$

$$\frac{\partial V_{ax}}{\partial C} = s_x \cdot g \cdot (-sinC_x cos\theta cos\varphi - cosA_x cosC_x (sin\phi cos\varphi + cos\phi sin\theta cos\varphi - sinA_x cosC_x (cos\phi sin\varphi - sin\phi sin\theta cos\varphi) \tag{A.3}$$

$$\frac{\partial V_{ax}}{\partial A} = s_x \cdot g \cdot (sinA_x sinC_x (sin\phi cos\varphi + cos\phi sin\theta cos\varphi) - cosA_x sinC_x (cos\phi sin\varphi - sin\phi sin\theta cos\varphi) \tag{A.4}$$

For y-axis accelerometer, partial derivatives are as follows.

$$\frac{\partial V_{ay}}{\partial B} = 1 \tag{A.5}$$

$$\frac{\partial V_{ay}}{\partial S} = g \cdot (-cosC_y (cos\phi sin\varphi - sin\phi sin\theta cos\varphi) + sinA_y sinC_y (sin\phi sin\varphi + cos\phi sin\theta cos\varphi) - cosA_y cosC_y cos\theta cos\varphi) \tag{A.6}$$

$$\frac{\partial V_{ay}}{\partial C} = s_y \cdot g \cdot (sinC_y (cos\phi sin\varphi - sin\phi sin\theta cos\varphi) + sinA_y cosC_y (sin\phi sin\varphi + cos\phi sin\theta cos\varphi) - cosA_y cosC_y cos\theta cos\varphi) \tag{A.7}$$

$$\frac{\partial V_{ay}}{\partial A} = (cosA_y sinC_y (sin\phi sin\varphi + cos\phi sin\theta cos\varphi) + sinA_y sinC_y cos\theta cos\varphi) \tag{A.8}$$

For z-axis accelerometer, partial derivatives are as follows.

$$\frac{\partial V_{az}}{\partial B} = 1 \tag{A.9}$$

$$\frac{\partial V_{az}}{\partial S} = g \cdot (cosC_z (sin\phi sin\varphi + cos\phi sin\theta cos\varphi) + cosA_z sinC_z (cos\phi sin\varphi - sin\phi sin\theta cos\varphi) + sinA_y sinC_y cos\theta cos\varphi) \tag{A.10}$$

$$\frac{\partial V_{az}}{\partial C} = s_z \cdot g \cdot (-sinC_z(sin\phi sin\varphi + cos\phi sin\theta cos\varphi) + cosA_z cosC_z(cos\phi sin\varphi - sin\phi sin\theta cos\varphi) + sinA_y cosC_y cos\theta cos\varphi) \quad (A.11)$$

$$\frac{\partial V_{az}}{\partial A} = s_z \cdot g \cdot (-sinA_z sinC_z(cos\phi sin\varphi - sin\phi sin\theta cos\varphi) + cosA_y sinC_y cos\theta cos\varphi) \quad (A.12)$$

For x-axis gyroscope, partial derivatives are as follows.

$$\frac{\partial V_{gx}}{\partial B} = 1 \quad (A.13)$$

$$\frac{\partial V_{gx}}{\partial S} = (\dot{\theta} sin\varphi + \dot{\phi} cos\varphi cos\theta) cosC_x + (\dot{\theta} cos\varphi - \dot{\phi} cos\theta sin\varphi) sinA_x sinC_x + (\dot{\varphi} + \dot{\phi} sin\theta) cosA_x sinC_x \quad (A.14)$$

$$\frac{\partial V_{gx}}{\partial C} = s_x \cdot (-(\dot{\theta} sin\varphi + \dot{\phi} cos\theta cos\varphi) sinC_x + (\dot{\theta} cos\varphi - \dot{\phi} cos\theta sin\varphi) sinA_x cosC_x - (\dot{\varphi} + \dot{\phi} sin\theta) cosA_x cosC_x) \quad (A.15)$$

$$\frac{\partial V_{gx}}{\partial A} = s_x \cdot ((\dot{\theta} cos\varphi - \dot{\phi} cos\theta sin\varphi) cosA_x sinC_x + (\dot{\varphi} + \dot{\phi} sin\theta) sinA_x sinC_x) \quad (A.16)$$

For y-axis gyroscope, partial derivatives are as follows.

$$\frac{\partial V_{gy}}{\partial B} = 1 \quad (A.17)$$

$$\frac{\partial V_{gy}}{\partial S} = (\dot{\theta} cos\dot{\varphi} - \dot{\phi} cos\theta sin\varphi) cosC_y - (\dot{\theta} sin\varphi + \dot{\phi} cos\theta cos\varphi) cosA_y cosC_y + (\dot{\varphi} + \dot{\phi} sin\theta) sinA_y sinC_y \quad (A.18)$$

$$\frac{\partial V_{gy}}{\partial C} = s_y \cdot (-(\dot{\theta} cos\dot{\varphi} - \dot{\phi} cos\theta sin\varphi) sinC_y - (\dot{\theta} sin\varphi + \dot{\phi} cos\theta cos\varphi) cosA_y cosC_y + (\dot{\varphi} + \dot{\phi} sin\theta) cosA_y sinC_y) \quad (A.19)$$

$$\frac{\partial V_{gy}}{\partial A} = s_x \cdot ((\dot{\theta} sin\varphi + \dot{\phi} cos\theta cos\varphi) sinA_y sinC_y + (\dot{\varphi} + \dot{\phi} sin\theta) cosA_y sinC_y) \quad (A.20)$$

For z-axis gyroscope, partial derivatives are as follows.

$$\frac{\partial V_z}{\partial B} = 1 \quad (A.21)$$

$$\frac{\partial V_{gz}}{\partial S} = (\dot{\varphi} + \dot{\phi} sin\theta) cosC_z - (\dot{\theta} cos\varphi - \dot{\phi} cos\theta sin\varphi) cosA_z sinC_z + (\dot{\theta} sin\varphi + \dot{\phi} cos\theta cos\varphi) sinA_z sinC_z \quad (A.22)$$

$$\frac{\partial V_{gz}}{\partial C} = s_z \cdot (-(\dot{\varphi} + \dot{\phi} sin\theta) sinC_z - (\dot{\theta} cos\varphi - \dot{\phi} cos\theta sin\varphi) cosA_z cosC_z + (\dot{\theta} sin\varphi + \dot{\phi} cos\theta cos\varphi) sinA_z cosC_z) \quad (A.23)$$

$$\frac{\partial V_{gz}}{\partial A} = s_z \cdot ((\dot{\theta} cos\varphi - \dot{\phi} cos\theta sin\varphi) sinA_z sinC_z + (\dot{\theta} sin\varphi + \dot{\phi} cos\theta cos\varphi) cosA_z sinC_z) \quad (A.24)$$

The initial parameter values used in the simulation are experiment given in Table A.1. There is no special reason for selecting different values in accelerometers and gyroscopes.

Table A.1 Initial parameter values for simulation and experiment

parameters	accelerometer	gyroscope
simulation and experiment		
bias [g]/[rad/s]	0.02000	0.01744
sensitivity	1.02000	1.00350
coning angle [rad]	0.03488	0.01744
azimuth angle [rad]	0.03488	0.03488